

# Boreal–Arctic wetland methane emissions modulated by warming and vegetation activity

Received: 12 June 2023

Accepted: 19 January 2024

Published online: 14 February 2024

 Check for updates

Kunxiaoja Yuan<sup>1,7</sup>, Fa Li<sup>2,7</sup>, Gavin McNicol<sup>3</sup>, Min Chen<sup>2</sup>, Alison Hoyt<sup>4</sup>, Sara Knox<sup>5,6</sup>, William J. Riley<sup>1</sup>, Robert Jackson<sup>4</sup> & Qing Zhu<sup>1</sup>✉

Wetland methane (CH<sub>4</sub>) emissions over the Boreal–Arctic region are vulnerable to climate change and linked to climate feedbacks, yet understanding of their long-term dynamics remains uncertain. Here, we upscaled and analysed two decades (2002–2021) of Boreal–Arctic wetland CH<sub>4</sub> emissions, representing an unprecedented compilation of eddy covariance and chamber observations. We found a robust increasing trend of CH<sub>4</sub> emissions (+8.9%) with strong inter-annual variability. The majority of emission increases occurred in early summer (June and July) and were mainly driven by warming (52.3%) and ecosystem productivity (40.7%). Moreover, a 2 °C temperature anomaly in 2016 led to the highest recorded annual CH<sub>4</sub> emissions (22.3 Tg CH<sub>4</sub> yr<sup>-1</sup>) over this region, driven primarily by high emissions over Western Siberian lowlands. However, current-generation models from the Global Carbon Project failed to capture the emission magnitude and trend, and may bias the estimates in future wetland CH<sub>4</sub> emission driven by amplified Boreal–Arctic warming and greening.

Methane (CH<sub>4</sub>) contributes approximately 20–30% of global emission-related radiative forcing<sup>1,2</sup>, and is the second largest source of current anthropogenic warming, with a global warming potential 28–34 times larger than that of CO<sub>2</sub> over a 100-year time horizon<sup>1,3</sup>. Wetlands are the largest and most uncertain natural source of global CH<sub>4</sub> emissions<sup>4–6</sup> and wetland CH<sub>4</sub> emissions are closely linked to temperature<sup>7–9</sup>. In a substantial portion of the Boreal–Arctic (that is, including northern boreal and tundra ecoregions and also areas north of 50° characterized by rock and ice<sup>10,11</sup>), recently observed warming has been occurring three to four times faster than the global average<sup>12</sup>, and has fuelled concerns given the positive feedbacks between CH<sub>4</sub> emissions and warming<sup>9,13,14</sup>. However, the regional response of Boreal–Arctic wetland CH<sub>4</sub> emissions to long-term environmental change remains unknown.

Warming<sup>15</sup> and increasing substrate availability for soil microbes due to an observed increase in vegetation productivity<sup>16</sup> should increase CH<sub>4</sub> production<sup>17,18</sup>, all else being equal. However, warming enhances aerobic<sup>19</sup> and anaerobic CH<sub>4</sub> oxidation<sup>20</sup>, and variations in inundation areas<sup>21,22</sup> could offset increased CH<sub>4</sub> production. In the Boreal–Arctic region, both positive and negative trends have been reported with top-down (TD; that is, atmospheric transport inversion) and bottom-up (BU; that is, using terrestrial ecosystem models) approaches<sup>17,18,23</sup> due to several sources of uncertainty, including parameterization of biogeochemical processes<sup>17,18</sup>, representation of atmospheric transport and photochemical sinks<sup>6,24,25</sup>, wetland inundation dynamics<sup>6,21</sup> and limited ground observations<sup>6,26,27</sup>.

The magnitude of Boreal–Arctic regional wetland CH<sub>4</sub> emissions also remains highly uncertain<sup>6,24,28–31</sup>, with previous estimates ranging

<sup>1</sup>Climate and Ecosystem Sciences Division, Climate Sciences Department, Lawrence Berkeley National Laboratory, Berkeley, CA, USA. <sup>2</sup>Department of Forest and Wildlife Ecology, University of Wisconsin Madison, Madison, WI, USA. <sup>3</sup>Department of Earth and Environmental Sciences, University of Illinois Chicago, Chicago, IL, USA. <sup>4</sup>Department of Earth System Science, Stanford University, Stanford, CA, USA. <sup>5</sup>Department of Geography, The University of British Columbia, Vancouver, British Columbia, Canada. <sup>6</sup>Department of Geography, McGill University, Montreal, Quebec, Canada. <sup>7</sup>These authors contributed equally: Kunxiaoja Yuan, Fa Li. ✉e-mail: [qzhu@lbl.gov](mailto:qzhu@lbl.gov)

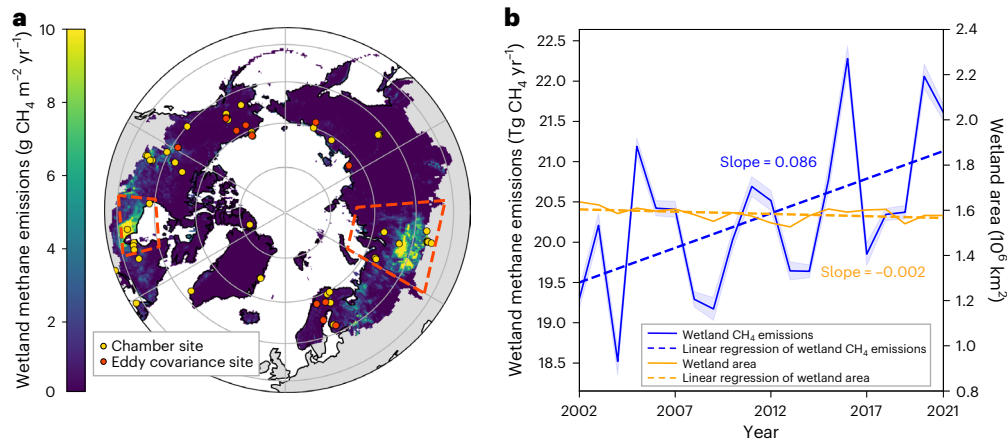


**Fig. 1 | Significant increasing trend of wetland CH<sub>4</sub> emissions in the Boreal-Arctic during 2002–2021.** **a**, Spatial distribution of the long-term averaged wetland CH<sub>4</sub> emissions in the Boreal-Arctic upscaled by combining chamber and EC datasets. Red dashed boxes indicate two wetland hotspots: WSL (52–74° N, 60–94.5° E) and HBL (50–60° N, 75–96° W). Boreal-Arctic basemap data from ref. 72. **b**, Annual Boreal-Arctic wetland CH<sub>4</sub> emissions and Wetland Area and

Dynamics for Methane Modeling (WAD2M) wetland area dataset between 2002 and 2021. Dashed lines indicate the linear regression results for wetland CH<sub>4</sub> emissions ( $P = 0.017$ , two-sided  $t$ -test) and wetland area ( $P = 0.064$ ). The blue shaded area indicates the s.d. in estimated wetland CH<sub>4</sub> variability due to model parameter uncertainty.

from about 9 to 53 Tg CH<sub>4</sub> yr<sup>-1</sup> (refs. 6,28,32–39). Although current TD models generally agreed on higher emissions relative to BU models during 2008–2017<sup>5</sup>, the uncertainty ranges within both BU and TD models exceeded the magnitude of CH<sub>4</sub> emissions they estimated. Notably, the uncertainty of the Boreal-Arctic wetland CH<sub>4</sub> emissions is twice as large as the global atmospheric CH<sub>4</sub> changes due to a sink–source imbalance of -20 Tg CH<sub>4</sub> yr<sup>-1</sup> (ref. 25), limiting reliable conclusions on natural and anthropogenic fluxes for the global CH<sub>4</sub> budget<sup>6,24,25</sup>.

Narrowing these substantial uncertainties in estimates of regional wetland CH<sub>4</sub> emissions requires better understanding and model representations of the relationships between wetland CH<sub>4</sub> emissions and environmental drivers. Previous meta-analyses have revealed a dependence of CH<sub>4</sub> emissions on temperature from methanogen cultures to ecosystem scales<sup>9</sup>. Existing observations have also demonstrated confounding effects on CH<sub>4</sub> emissions from other factors, including hydrologic and vegetation conditions<sup>7,8,40,41</sup>, microbial dynamics and composition<sup>42,43</sup> and substrate availability<sup>44</sup>. Additionally, the relationships between CH<sub>4</sub> emissions and environmental drivers show substantial hysteresis, hypothesized to result from time lags between primary productivity and its conversion to methanogenesis substrates<sup>45</sup> and interactions between fermentation, acetate availability and acetoclastic methanogen biomass and activity<sup>46</sup>. These effects could largely modulate the timing and magnitude of CH<sub>4</sub> emissions<sup>7,8,13,45,47</sup> and affect model estimates<sup>7,13,28</sup>, yet they have not been explicitly considered when exploring the responses of the Boreal-Arctic wetlands to climate change.

Furthermore, Boreal-Arctic wetland CH<sub>4</sub> emissions exhibit strong spatial heterogeneity<sup>7,41,48</sup> and temporal variability<sup>17,27,48</sup>, highlighting the need for widespread flux observations to constrain models<sup>27</sup>. Existing eddy covariance (EC) measurements within the FLUXNET-CH<sub>4</sub> network<sup>26,27</sup> (Fig. 1a, red circles) over the Boreal-Arctic have been distributed over non-hotspot wetlands since 2006 (Supplementary Fig. 1a), while chamber observations (Fig. 1a, yellow circles) are available beyond EC-observed years and in wetland hotspots, that is, the Western Siberian lowlands (WSL) and Hudson Bay lowlands (HBL). Combining EC and chamber measurements thus provides expanded spatial and temporal coverage of observational constraints, albeit with challenges in reconciling the two kinds of datum with different spatial and temporal scales<sup>27</sup>.

Here, we quantified the decadal responses of wetland CH<sub>4</sub> emissions to environmental changes in the Boreal-Arctic region by considering the lagged dependence of CH<sub>4</sub> emissions on abiotic and biotic

drivers and using the largest dataset of the Boreal-Arctic CH<sub>4</sub> compiled to date, which combines both EC tower and chamber data (Methods). The CH<sub>4</sub> emission dataset has 139 and 168 site years of EC and chamber measurements, respectively, sampled in both hotspot and non-hotspot regions (Fig. 1a). We generated an upscaled data product of Boreal-Arctic wetland CH<sub>4</sub> emissions during 2002–2021 using a physically interpretable and causality-guided machine learning model<sup>7</sup>. Specifically, the causal relationships between CH<sub>4</sub> emission and its drivers inferred from observations (Methods) were used to guide model training, achieving higher accuracy than commonly used machine learning methods<sup>7</sup>. Using the upscaled dataset, we investigated the predominant drivers that regulate the long-term trend and variability of CH<sub>4</sub> emissions. We also benchmarked the performance of BU ( $n = 13$ ) and TD ( $n = 21$ ) models that participated in the most recent Global Carbon Project – CH<sub>4</sub> budget<sup>6,24</sup>.

## Multidecadal temporal dynamics of wetland CH<sub>4</sub> emissions

The upscaled Boreal-Arctic wetland CH<sub>4</sub> emission dataset revealed that the mean annual emissions were  $20.3 \pm 0.9$  (mean  $\pm$  1 s.d.) Tg CH<sub>4</sub> yr<sup>-1</sup> from 2002 to 2021, where -53% of the total was contributed by the two hotspot areas (Fig. 1a, regions highlighted in the red boxes). Specifically, the largest hotspot was the WSL, which emitted  $6.6 \pm 0.5$  Tg CH<sub>4</sub> yr<sup>-1</sup>, ~57% larger than the second hotspot, the HBL ( $4.2 \pm 0.3$  Tg CH<sub>4</sub> yr<sup>-1</sup>). The upscaled CH<sub>4</sub> emissions were validated against randomly excluded site observations (Methods), and the Pearson correlation coefficient ( $R$ ), mean absolute error and normalized mean absolute error between estimated and measured CH<sub>4</sub> emissions were  $0.89 \pm 0.02$ ,  $20.81 \pm 1.88$  nmol CH<sub>4</sub> m<sup>-2</sup> s<sup>-1</sup> and  $3.65 \pm 0.50\%$  (Supplementary Fig. 2), respectively. Detailed information for the observation sites is found in Supplementary Tables 1 and 2.

Furthermore, a significant increasing trend ( $P < 0.05$ ) of the Boreal-Arctic CH<sub>4</sub> emissions was detected from 2002 to 2021 (Fig. 1b, blue line). The trend revealed an -8.9% increase in CH<sub>4</sub> emissions since 2002. The WSL and non-hotspot regions contributed -56% and -38% of the increasing trend, respectively, while no significant trend was found in the HBL (Supplementary Fig. 3). The CH<sub>4</sub> emission enhancement during the boreal summer (June–August) contributed the most (-76%) to the annual-scale increasing trend (Supplementary Fig. 4), with -62% of the increase occurring during early boreal summer (June and July). Previous observational work at a Siberian tundra site also documented

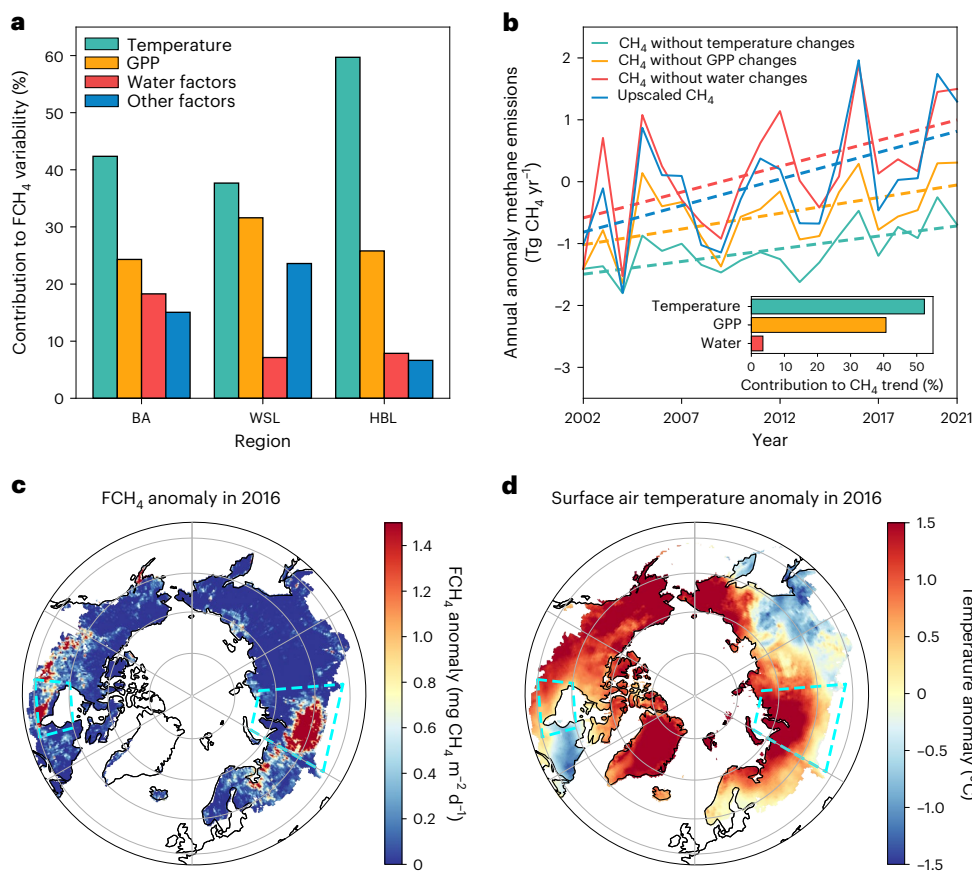


**Fig. 2 | Temperature dominated the variability and trend of wetland CH<sub>4</sub> emissions, and triggered the peak CH<sub>4</sub> emissions in 2016.** **a**, Contribution of abiotic and biotic drivers to wetland CH<sub>4</sub> flux (FCH<sub>4</sub>) variability in the Boreal–Arctic (BA), WSL and HBL, represented as the percentage of grids where wetland FCH<sub>4</sub> variability is dominated by temperature, GPP, water-related drivers (soil moisture content, and precipitation) and other drivers. **b**, Upscaled CH<sub>4</sub> emission annual anomalies (solid lines) and trends (dashed lines) using all drivers and

iteratively excluding the temporal dynamics for each group of drivers. Inset: contributions of different drivers to the CH<sub>4</sub> emission trend (Methods). **c,d**, CH<sub>4</sub> emission anomalies calculated relative to the multiyear annual-mean CH<sub>4</sub> emissions from 2002 to 2021: anomaly of FCH<sub>4</sub> (**c**) and surface air temperature<sup>73</sup> (**d**) in the peak emission year of 2016. The regions marked with dashed boxes are two wetland hotspots: WSL and HBL.

a long-term increasing trend of CH<sub>4</sub> emissions due to warming-induced early onset of snowmelt and vegetation growth<sup>49</sup>. We show here robust evidence of an increasing trend in the Boreal–Arctic region’s early summer CH<sub>4</sub> emissions.

Another line of evidence for the long-term increasing trend of the Boreal–Arctic wetland CH<sub>4</sub> emissions is the widespread increases in high-latitude atmospheric CH<sub>4</sub> concentrations observed from the National Oceanic and Atmospheric Administration (NOAA) Global Greenhouse Gas Reference Network<sup>50</sup>. All high-latitude stations (18 in total, Supplementary Fig. 1b) exhibited positive trends in observed atmospheric CH<sub>4</sub>, and the trends of all but one station were statistically significant ( $P < 0.05$ ) (Supplementary Table 3). Wetlands could be the dominant source of high-latitude CH<sub>4</sub> emissions compared with other sources<sup>6</sup>, particularly in the boreal summer months<sup>51</sup>. The increases in atmospheric CH<sub>4</sub> concentrations therefore probably reflect the increases in CH<sub>4</sub> emissions from wetlands.

### Drivers of wetland CH<sub>4</sub> emission variability and trend

Since no long-term increasing changes in wetland area were found over the Boreal–Arctic region<sup>21</sup> during the past two decades (Fig. 1b, yellow line), our results suggested that the increasing trend of regional wetland CH<sub>4</sub> emissions was induced primarily by changes in CH<sub>4</sub> emission intensity rather than expansion of total wetland area. After accounting for confounding effects from other abiotic and biotic factors (Methods),

temperature was identified as the predominant control on wetland CH<sub>4</sub> emission variability over the Boreal–Arctic (Fig. 2b). Specifically, temperature dominated the variability in most grid cells (42.4%), followed by gross primary productivity (GPP) (24.3%), while water-related factors (soil water content, and precipitation) dominated the other 18.3% of grid cells. Consistent patterns of the predominant drivers were also found in the two wetland hotspots, and the grid cells with wetland CH<sub>4</sub> flux observations. About 37.7%, 59.7% and 61.3% of grid cells were dominated by temperature in the WSL, HBL and the full observation-covered area, respectively (Fig. 2a and Supplementary Fig. 5). Temperature is closely linked to wetland CH<sub>4</sub> production and emissions, while GPP could be a proxy for substrate availability and plant-mediated CH<sub>4</sub> transport<sup>7,8,47</sup>. The dominance of temperature and GPP effects is consistent with previous studies<sup>7,8,41,47</sup>, implying a potential sensitivity of wetland CH<sub>4</sub> emissions to warming and vegetation activities<sup>52</sup>.

For potential drivers of the Boreal–Arctic wetland CH<sub>4</sub> emission trend, we used a statistical model (Methods)<sup>53,54</sup> to partition the contributions from various factors including temperature, vegetation activities and water conditions. We found that in the Boreal–Arctic (Fig. 2b) temperature explained 52.3% of the increasing CH<sub>4</sub> emission trend, followed by GPP (40.7%). In the Boreal–Arctic, significant increases in temperature<sup>12</sup> and GPP<sup>52,55</sup> have been detected using satellite-based products. While warming can increase both wetland CH<sub>4</sub> production and oxidation in observations<sup>19,20</sup> and model simulations<sup>56</sup>,

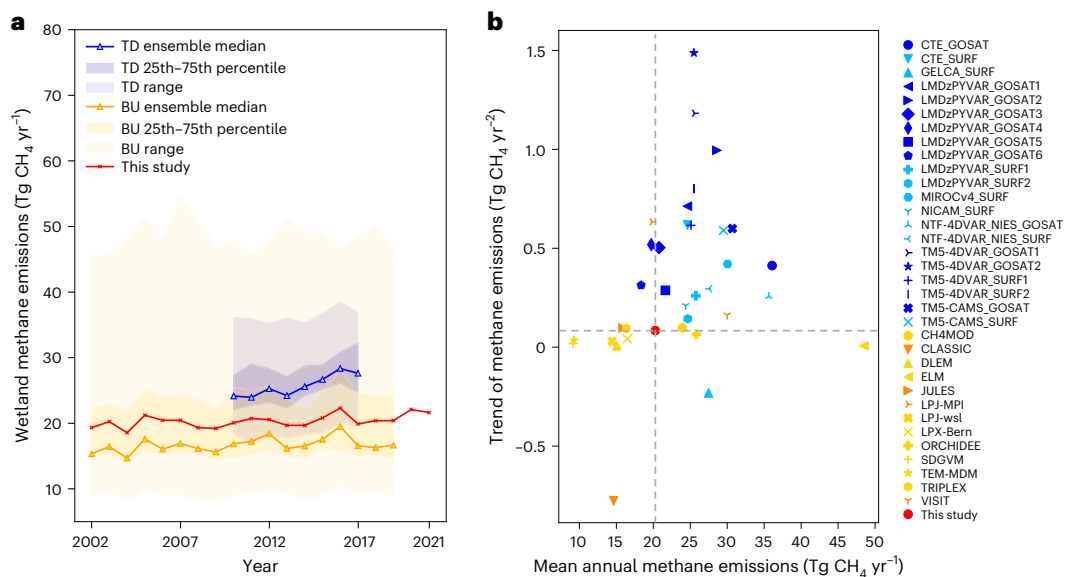


**Fig. 3 | BU and TD models exhibited substantial uncertainties in the magnitude and trend of wetland CH<sub>4</sub> emissions over the Boreal–Arctic region. a**, The multimodel ensemble median (50th percentile) of wetland CH<sub>4</sub> emissions estimated by TD (blue line) and BU (orange line) models, compared with the upscaled wetland CH<sub>4</sub> emissions (red line). The darker shaded areas represent 25th to 75th percentiles and the lighter shaded areas represent the ranges of wetland CH<sub>4</sub> emissions. **b**, The mean annual magnitudes and trends of

wetland CH<sub>4</sub> emissions estimated by TD and BU models, compared with those of the upscaled wetland CH<sub>4</sub> emissions (red circle). For TD models, dark-blue markers indicate that the trends are significant, that is,  $P < 0.05$ , and light-blue markers indicate that the trends are not significant, that is,  $P > 0.05$ . For BU models, orange markers indicate that the trends are significant, and yellow markers indicate that the trends are not significant. The  $P$  values can be seen in Supplementary Table 5, obtained from a two-sided  $t$ -test.

our analysis here revealed net positive effects of temperature on CH<sub>4</sub> emissions. Meanwhile, warming has also increased vegetation productivity in the Boreal–Arctic<sup>52</sup>, which could promote plant-mediated CH<sub>4</sub> transport via aerenchyma tissue and increase organic substrate supply for microbes. The increase of substrate availability could fuel methanogens<sup>57–59</sup>, leading to an increase in wetland CH<sub>4</sub> emissions<sup>49</sup>.

Given the dominant control of temperature on wetland CH<sub>4</sub> emissions, high CH<sub>4</sub> emissions can be triggered by abnormally high temperatures over high-emission wetlands. Anomalously high (2005, 2016 and 2020) and low (2004, 2009 and 2014) CH<sub>4</sub> emission years (Fig. 2b) had higher and lower annual-mean temperatures, respectively, particularly in the two CH<sub>4</sub> hotspot regions (Supplementary Figs. 6 and 7). The highest-emission year occurred in 2016 (Fig. 2c,d), which was the warmest year in the high latitudes since 1950<sup>12</sup>. The anomalously high temperature in 2016 was suggested to be caused by the major El Niño event during 2015–2016<sup>60,61</sup>. This strong El Niño event changed large-scale divergence and convergence patterns and upper-level moisture transport<sup>62</sup>, leading to subsequent changes in adiabatic warming over the Arctic surface<sup>61,63</sup>. The resultant high temperature happened to overlap with wetland hotspots (Fig. 2d) and induced a sharp increase (–15.5% higher emissions relative to 2002) in wetland CH<sub>4</sub> emissions, particularly over the WSL (Fig. 2c). All sites except one (covering 2016 and its adjacent years) agreed with anomalously high wetland CH<sub>4</sub> emissions in 2016 when the temperature was anomalously high (Supplementary Table 4). These results highlight the role of major El Niño–Southern Oscillation events in driving wetland CH<sub>4</sub> emission variability<sup>64–66</sup>, and demonstrate a critical ecological teleconnection from the sea surface temperature of the tropical Pacific to the Boreal–Arctic wetland CH<sub>4</sub> emissions.

### Implications for modelling wetland CH<sub>4</sub> emissions

Most of the current generation of BU and TD models in the Global Carbon Project CH<sub>4</sub> budget<sup>6</sup> did not capture the observed magnitude and trend of wetland CH<sub>4</sub> emissions in the Boreal–Arctic (Fig. 3a,b). For emission magnitude, 19 out of 21 TD models overestimated and 9 out of

13 BU models underestimated the Boreal–Arctic wetland CH<sub>4</sub> emissions when compared with our upscaled dataset (Fig. 3b, Supplementary Fig. 8 and Supplementary Table 5). The rest (4 of 13) of the BU models overestimated the Boreal–Arctic wetland CH<sub>4</sub> emissions by 18% to 139%, with the ensemble median of all BU models (16.66 Tg CH<sub>4</sub> yr<sup>-1</sup>) lower than that of the observationally constrained upscaled dataset (Fig. 3a). For the long-term trend, the majority (10 of 13) of BU models did not show the significantly increasing trend, while the other BU models with increasing trends differed by up to sixfold in trend magnitude relative to the upscaled trend. More (12 of 21) TD models exhibited significant increasing trends, but the trend magnitude differed by a factor ranging from 2 to 16 (Supplementary Table 5).

The lack of increasing trends in most of the current-generation process-based biogeochemical models suggests probable underestimation of future warming-induced increases in wetland CH<sub>4</sub> emissions. Future Boreal–Arctic warming could further increase the intensity of wetland CH<sub>4</sub> emissions and stimulate a large increase in wetland extent due to permafrost thaw<sup>14</sup> and greater precipitation<sup>67</sup>. The underestimated increasing trend indicates that the BU model underestimated intensity in wetland emissions rather than wetland extent since all models prescribed the same wetland extent data<sup>21</sup> with no significant temporal changes in wetland area (Fig. 1b). The underestimated intensity of CH<sub>4</sub> emissions therefore could be multiplied by future expanded wetland area, leading to amplified underestimation of wetland CH<sub>4</sub> emissions and their positive feedbacks with warming. The upscaling models showed good performance and confirmed the increasing wetland CH<sub>4</sub> emission trend in the Boreal–Arctic during 2002–2021, even considering the uncertainties from which site observations were used and validation schemes (Supplementary Fig. 9), wetland extent (Supplementary Fig. 10a) and input variables (Supplementary Fig. 10b). The increasing wetland CH<sub>4</sub> emissions in the high latitudes indicate the growingly important role of biogenic CH<sub>4</sub> emissions in rising atmospheric CH<sub>4</sub><sup>68–70</sup>. Underrating the upward trend of wetland CH<sub>4</sub> emissions, therefore, suggests underestimated biogenic contributions to observed increases in atmospheric CH<sub>4</sub> and radiative forcing<sup>25</sup>.



Our data-driven, long-term and spatially explicit wetland CH<sub>4</sub> emission dataset opens up new opportunities to better understand the dynamics of the Boreal–Arctic wetland CH<sub>4</sub> emissions and could facilitate the improvement of BU and TD models. The upscaled dataset is well constrained by widespread observations, particularly during the summer season (Supplementary Tables 1 and 2) when the major increasing trend of wetland CH<sub>4</sub> emissions was reported. The dataset also explicitly considers the frequently acknowledged but under-represented hysteresis characteristics in wetland CH<sub>4</sub> emissions<sup>7,8,13</sup>. We demonstrated the dominant controls of temperature and GPP on the CH<sub>4</sub> emission trend and variability, suggesting the priority of refining CH<sub>4</sub> emission temperature sensitivity and plant-modulated CH<sub>4</sub> emission processes in BU models. For example, the temperature dependence of CH<sub>4</sub> emissions has been empirically represented and poorly parameterized in biogeochemical models<sup>13</sup>. Plant-mediated microbial substrate availability is strongly linked to CH<sub>4</sub> emissions<sup>57</sup>, yet has rarely been mechanistically represented in models<sup>13</sup>. Current biogeochemical models have little consensus on model structure or complexity in representing wetland CH<sub>4</sub> emissions<sup>71</sup>. Confidence in model predictions is limited by knowledge gaps and ability to validate models across time and space. This new benchmark dataset could aid validation and parameterizations of the highly uncertain biogeochemical processes related to CH<sub>4</sub> emissions. Additionally, the upscaled dataset provides better prior information for TD transport inversion models, thereby allowing for more reliable separation of natural and anthropogenic CH<sub>4</sub> emission effects on atmospheric CH<sub>4</sub> concentrations.

### Online content

Any methods, additional references, Nature Portfolio reporting summaries, source data, extended data, supplementary information, acknowledgements, peer review information; details of author contributions and competing interests; and statements of data and code availability are available at <https://doi.org/10.1038/s41558-024-01933-3>.

### References

- Bergamaschi, P. et al. Atmospheric CH<sub>4</sub> in the first decade of the 21st century: inverse modeling analysis using SCIAMACHY satellite retrievals and NOAA surface measurements. *J. Geophys. Res. Atmos.* **118**, 7350–7369 (2013).
- Ciais, P. et al. Carbon and other biogeochemical cycles. in *Climate Change 2013: The Physical Science Basis. Contribution of Working Group I to the Fifth Assessment Report of the Intergovernmental Panel on Climate Change* (eds Stocker, T. F. et al.) Ch. 6 (Cambridge Univ. Press, 2013).
- Neubauer, S. C. & Megonigal, J. P. Moving beyond global warming potentials to quantify the climatic role of ecosystems. *Ecosystems* **18**, 1000–1013 (2015).
- Bousquet, P. et al. Contribution of anthropogenic and natural sources to atmospheric methane variability. *Nature* **443**, 439–443 (2006).
- Chen, Y. H. & Prinn, R. G. Estimation of atmospheric methane emissions between 1996 and 2001 using a three-dimensional global chemical transport model. *J. Geophys. Res. Atmos.* **111**, D10 (2006).
- Saunois, M. et al. The global methane budget 2000–2017. *Earth Syst. Sci. Data* **12**, 1561–1623 (2020).
- Yuan, K. et al. Causality guided machine learning model on wetland CH<sub>4</sub> emissions across global wetlands. *Agric. Meteorol.* **324**, 109115 (2022).
- Knox, S. H. et al. Identifying dominant environmental predictors of freshwater wetland methane fluxes across diurnal to seasonal time scales. *Glob. Change Biol.* **27**, 3582–3604 (2021).
- Yvon-Durocher, G. et al. Methane fluxes show consistent temperature dependence across microbial to ecosystem scales. *Nature* **507**, 488–491 (2014).
- Olson, D. M. et al. Terrestrial ecoregions of the world: a new map of life on Earth: a new global map of terrestrial ecoregions provides an innovative tool for conserving biodiversity. *BioScience* **51**, 933–938 (2001).
- Olefeldt, D. et al. The Boreal–Arctic Wetland and Lake Dataset (BAWLD). *Earth Syst. Sci. Data* **13**, 5127–5149 (2021).
- Rantanen, M. et al. The Arctic has warmed nearly four times faster than the globe since 1979. *Commun. Earth Environ.* **3**, 168 (2022).
- Chang, K.-Y. et al. Substantial hysteresis in emergent temperature sensitivity of global wetland CH<sub>4</sub> emissions. *Nat. Commun.* **12**, 2266 (2021).
- Zhang, Z. et al. Emerging role of wetland methane emissions in driving 21st century climate change. *Proc. Natl Acad. Sci. USA* **114**, 9647–9652 (2017).
- Jerman, V., Metje, M., Mandić-Mulec, I. & Frenzel, P. Wetland restoration and methanogenesis: the activity of microbial populations and competition for substrates at different temperatures. *Biogeosciences* **6**, 1127–1138 (2009).
- Chen, M. et al. Regional contribution to variability and trends of global gross primary productivity. *Environ. Res. Lett.* **12**, 105005 (2017).
- Poulter, B. et al. Global wetland contribution to 2000–2012 atmospheric methane growth rate dynamics. *Environ. Res. Lett.* **12**, 094013 (2017).
- Ito, A. Methane emission from pan-Arctic natural wetlands estimated using a process-based model, 1901–2016. *Polar Sci.* **21**, 26–36 (2019).
- Dean, J. F. et al. Methane feedbacks to the global climate system in a warmer world. *Rev. Geophys.* **56**, 207–250 (2018).
- Segarra, K. et al. High rates of anaerobic methane oxidation in freshwater wetlands reduce potential atmospheric methane emissions. *Nat. Commun.* **6**, 7477 (2015).
- Zhang, Z. et al. Development of the global dataset of Wetland Area and Dynamics for Methane Modeling (WAD2M). *Earth Syst. Sci. Data* **13**, 2001–2023 (2021).
- Zhuang, Q. et al. Influence of changes in wetland inundation extent on net fluxes of carbon dioxide and methane in northern high latitudes from 1993 to 2004. *Environ. Res. Lett.* **10**, 095009 (2015).
- Stavert, A. R. et al. Regional trends and drivers of the global methane budget. *Glob. Change Biol.* **28**, 182–200 (2022).
- Saunois, M. et al. The global methane budget 2000–2012. *Earth Syst. Sci. Data* **8**, 697–751 (2016).
- Turner, A. J., Frankenberg, C. & Kort, E. A. Interpreting contemporary trends in atmospheric methane. *Proc. Natl Acad. Sci. USA* **116**, 2805–2813 (2019).
- Delwiche, K. B. et al. FLUXNET-CH<sub>4</sub>: a global, multi-ecosystem dataset and analysis of methane seasonality from freshwater wetlands. *Earth Syst. Sci. Data* **13**, 3607–3689 (2021).
- Knox, S. H. et al. FLUXNET-CH<sub>4</sub> synthesis activity: objectives, observations, and future directions. *Bull. Am. Meteorol. Soc.* **100**, 2607–2632 (2019).
- Kuhn, M. A. et al. BAWLD-CH<sub>4</sub>: a comprehensive dataset of methane fluxes from boreal and arctic ecosystems. *Earth Syst. Sci. Data* **13**, 5151–5189 (2021).
- Arctic Monitoring and Assessment Programme (AMAP) *Impacts of Short-Lived Climate Forcers on Arctic Climate, Air Quality, and Human Health. Summary for Policy-Makers* (AMAP, 2021).
- Arctic Monitoring and Assessment Programme (AMAP) *Arctic Climate Change Update 2021: Key Trends and Impacts. Summary for Policy-Makers* (AMAP, 2021).
- Arctic Monitoring and Assessment Programme (AMAP) *AMAP Assessment 2015: Methane as an Arctic Climate Forcer* (AMAP, 2015).
- Spahni, R. et al. Constraining global methane emissions and uptake by ecosystems. *Biogeosciences* **8**, 1643–1665 (2011).

33. McGuire, A. et al. An assessment of the carbon balance of Arctic tundra: comparisons among observations, process models, and atmospheric inversions. *Biogeosciences* **9**, 3185–3204 (2012).
34. Zhu, X., Zhuang, Q., Qin, Z., Glagolev, M. & Song, L. Estimating wetland methane emissions from the northern high latitudes from 1990 to 2009 using artificial neural networks. *Glob. Biogeochem. Cycles* **27**, 592–604 (2013).
35. Bruhwiler, L. et al. CarbonTracker-CH<sub>4</sub>: an assimilation system for estimating emissions of atmospheric methane. *Atmos. Chem. Phys.* **14**, 8269–8293 (2014).
36. Treat, C. C., Bloom, A. A. & Marushchak, M. E. Nongrowing season methane emissions—a significant component of annual emissions across northern ecosystems. *Glob. Change Biol.* **24**, 3331–3343 (2018).
37. Watts, J. D., Kimball, J. S., Bartsch, A. & McDonald, K. C. Surface water inundation in the boreal–Arctic: potential impacts on regional methane emissions. *Environ. Res. Lett.* **9**, 075001 (2014).
38. Thompson, R. L. et al. Variability in atmospheric methane from fossil fuel and microbial sources over the last three decades. *Geophys. Res. Lett.* **45**, 11499–11508 (2018).
39. Peltola, O. et al. Monthly gridded data product of northern wetland methane emissions based on upscaling eddy covariance observations. *Earth Syst. Sci. Data* **11**, 1263–1289 (2019).
40. Olefeldt, D., Turetsky, M. R., Crill, P. M. & McGuire, A. D. Environmental and physical controls on northern terrestrial methane emissions across permafrost zones. *Glob. Change Biol.* **19**, 589–603 (2013).
41. Turetsky, M. R. et al. A synthesis of methane emissions from 71 northern, temperate, and subtropical wetlands. *Glob. Change Biol.* **20**, 2183–2197 (2014).
42. McCalley, C. K. et al. Methane dynamics regulated by microbial community response to permafrost thaw. *Nature* **514**, 478–481 (2014).
43. Oh, Y. et al. Reduced net methane emissions due to microbial methane oxidation in a warmer Arctic. *Nat. Clim. Change* **10**, 317–321 (2020).
44. Bergman, I., Klarqvist, M. & Nilsson, M. Seasonal variation in rates of methane production from peat of various botanical origins: effects of temperature and substrate quality. *FEMS Microbiol. Ecol.* **33**, 181–189 (2000).
45. Rinne, J. et al. Temporal variation of ecosystem scale methane emission from a boreal fen in relation to temperature, water table position, and carbon dioxide fluxes. *Glob. Biogeochem. Cycles* **32**, 1087–1106 (2018).
46. Chang, K.-Y., Riley, W. J., Crill, P. M., Grant, R. F. & Saleska, S. R. Hysteretic temperature sensitivity of wetland CH<sub>4</sub> fluxes explained by substrate availability and microbial activity. *Biogeosciences* **17**, 5849–5860 (2020).
47. Sturtevant, C. et al. Identifying scale-emergent, nonlinear, asynchronous processes of wetland methane exchange. *J. Geophys. Res. Biogeosci.* **121**, 188–204 (2016).
48. Bao, T., Jia, G. & Xu, X. Wetland heterogeneity determines methane emissions: a pan-Arctic synthesis. *Environ. Sci. Technol.* **55**, 10152–10163 (2021).
49. Röbger, N., Sachs, T., Wille, C., Boike, J. & Kutzbach, L. Seasonal increase of methane emissions linked to warming in Siberian tundra. *Nat. Clim. Change* **12**, 1031–1036 (2022).
50. Sweeney, C. et al. Seasonal climatology of CO<sub>2</sub> across North America from aircraft measurements in the NOAA/ESRL Global Greenhouse Gas Reference Network. *J. Geophys. Res. Atmos.* **120**, 5155–5190 (2015).
51. Nisbet, E. G., Dlugokencky, E. J. & Bousquet, P. Methane on the rise—again. *Science* **343**, 493–495 (2014).
52. Piao, S. et al. Characteristics, drivers and feedbacks of global greening. *Nat. Rev. Earth Environ.* **1**, 14–27 (2020).
53. Andela, N. & Van Der Werf, G. R. Recent trends in African fires driven by cropland expansion and El Niño to La Niña transition. *Nat. Clim. Change* **4**, 791–795 (2014).
54. Archibald, S., Nickless, A., Govender, N., Scholes, R. J. & Lehsten, V. Climate and the inter-annual variability of fire in southern Africa: a meta-analysis using long-term field data and satellite-derived burnt area data. *Glob. Ecol. Biogeogr.* **19**, 794–809 (2010).
55. Yang, R. et al. Divergent historical GPP trends among state-of-the-art multi-model simulations and satellite-based products. *Earth Syst. Dyn.* **13**, 833–849 (2022).
56. Melton, J. et al. Present state of global wetland extent and wetland methane modelling: conclusions from a model inter-comparison project (WETCHIMP). *Biogeosciences* **10**, 753–788 (2013).
57. Mitra, B. et al. Spectral evidence for substrate availability rather than environmental control of methane emissions from a coastal forested wetland. *Agric. For. Meteorol.* **291**, 108062 (2020).
58. Ström, L., Tagesson, T., Mastepanov, M. & Christensen, T. R. Presence of *Eriophorum scheuchzeri* enhances substrate availability and methane emission in an Arctic wetland. *Soil Biol. Biochem.* **45**, 61–70 (2012).
59. Whiting, G. J. & Chanton, J. Primary production control of methane emission from wetlands. *Nature* **364**, 794–795 (1993).
60. Hu, S. & Fedorov, A. V. The extreme El Niño of 2015–2016 and the end of global warming hiatus. *Geophys. Res. Lett.* **44**, 3816–3824 (2017).
61. Jeong, H., Park, H.-S., Stuecker, M. F. & Yeh, S.-W. Distinct impacts of major El Niño events on Arctic temperatures due to differences in eastern tropical Pacific sea surface temperatures. *Sci. Adv.* **8**, eab18278 (2022).
62. Park, K., Kang, S. M., Kim, D., Stuecker, M. F. & Jin, F.-F. Contrasting local and remote impacts of surface heating on polar warming and amplification. *J. Clim.* **31**, 3155–3166 (2018).
63. Ding, Q. et al. Tropical forcing of the recent rapid Arctic warming in northeastern Canada and Greenland. *Nature* **509**, 209–212 (2014).
64. Zhang, Z. et al. Enhanced response of global wetland methane emissions to the 2015–2016 El Niño–Southern Oscillation event. *Environ. Res. Lett.* **13**, 074009 (2018).
65. Zhu, Q. et al. Interannual variation in methane emissions from tropical wetlands triggered by repeated El Niño Southern Oscillation. *Glob. Change Biol.* **23**, 4706–4716 (2017).
66. Hodson, E., Poulter, B., Zimmermann, N. E., Prigent, C. & Kaplan, J. O. The El Niño–Southern Oscillation and wetland methane interannual variability. *Geophys. Res. Lett.* **38**, L08810 (2011).
67. Cook, B. I. et al. Twenty-first century drought projections in the CMIP6 forcing scenarios. *Earth's Future* **8**, e2019EF001461 (2020).
68. Nisbet, E. et al. Rising atmospheric methane: 2007–2014 growth and isotopic shift. *Glob. Biogeochem. Cycles* **30**, 1356–1370 (2016).
69. Bloom, A. A., Palmer, P. I., Fraser, A., Reay, D. S. & Frankenberg, C. Large-scale controls of methanogenesis inferred from methane and gravity spaceborne data. *Science* **327**, 322–325 (2010).
70. Peng, S. et al. Wetland emission and atmospheric sink changes explain methane growth in 2020. *Nature* **612**, 477–482 (2022).
71. Wania, R. et al. Present state of global wetland extent and wetland methane modelling: methodology of a model intercomparison project (WETCHIMP). *Geosci. Model Dev. Discuss.* **5**, 4071–4136 (2012).
72. Olefeldt, D. et al. *The Fractional Land Cover Estimates from the Boreal-Arctic Wetland and Lake Dataset (BAWLD)*, 2021 (Arctic Data Center, accessed 1 June 2022); <https://arcticdata.io/catalog/view/doi:10.18739/A2C824F9X>

73. Muñoz-Sabater, J. et al. ERA5-Land: a state-of-the-art global reanalysis dataset for land applications. *Earth Syst. Sci. Data* **13**, 4349–4383 (2021).

**Publisher's note** Springer Nature remains neutral with regard to jurisdictional claims in published maps and institutional affiliations.

**Open Access** This article is licensed under a Creative Commons Attribution 4.0 International License, which permits use, sharing, adaptation, distribution and reproduction in any medium or format, as long as you give appropriate credit to the original author(s) and the

source, provide a link to the Creative Commons license, and indicate if changes were made. The images or other third party material in this article are included in the article's Creative Commons license, unless indicated otherwise in a credit line to the material. If material is not included in the article's Creative Commons license and your intended use is not permitted by statutory regulation or exceeds the permitted use, you will need to obtain permission directly from the copyright holder. To view a copy of this license, visit <http://creativecommons.org/licenses/by/4.0/>.

© The Author(s) 2024

## Methods

### Wetland datasets

We used the WAD2M dataset<sup>21</sup> derived from active and passive microwave remote sensing as the prescribed wetland extent. When compared with the optical-sensor-based products, the microwave-sensor-based WAD2M product can identify water conditions below vegetation canopies; the product also mitigated the risks of double counting wetland and water bodies in the Boreal–Arctic region by fusing multisource wetland extent datasets<sup>21</sup>. A promising capability of the WAD2M dataset is its ability to capture the inter-annual variations of wetland extent<sup>21</sup>. In addition to inundation dynamics, clear differences in the magnitude and processes of wetland CH<sub>4</sub> emissions have been reported across different wetland types<sup>7,8,41,47</sup>. Therefore, wetland types extracted from the Boreal–Arctic Wetland and Lake Dataset (BAWLD)<sup>11</sup> were used to separately model wetland CH<sub>4</sub> emissions across bogs, fens, marshes and tundra. The BAWLD dataset also avoided the double-counting problem<sup>11</sup>. All wetland grid cells in the BAWLD dataset that provided the wetland type information were considered for upscaling, and the wetland type percentage provided by the BAWLD dataset was used for partitioning the wetland extent of the corresponding grid cells in the WAD2M dataset for each wetland type (Supplementary Section 1).

In addition, we also used other wetland datasets, including static wetlands from the Global Lakes and Wetlands Database<sup>74</sup>, and temporally dynamic model-derived wetlands<sup>75</sup> calibrated by observations from Global Inundation Extent from Multi-Satellites<sup>76</sup> and Regularly Flooded Wetland<sup>77</sup>. We discussed the temporal changes of wetland CH<sub>4</sub> emissions in the Boreal–Arctic during 2002–2021 related to the uncertain wetland extent. More details of the three wetland datasets used and the sensitivity experiments are given in Supplementary Section 3.

### Input datasets

Temperature-, plant- and water-related variables that have been shown to be important for explaining wetland CH<sub>4</sub> dynamics were used as input drivers for upscaling<sup>7,8,41,47</sup>. Specifically, the input variables include soil temperature (TS), air temperature (TA), GPP, air pressure (PA), precipitation (P), wind speed (WS), snow cover (SC) and soil water content (SWC). GPP was obtained from the GOSIF dataset<sup>78</sup>, which was derived on the basis of solar-induced chlorophyll fluorescence (SIF) observed with the Orbiting Carbon Observatory-2 and its linear relationship with GPP<sup>79,80</sup>. Other variables were obtained from the land component of the fifth generation of European Reanalysis (ERA5-Land) datasets<sup>73</sup> because of the high accuracy and physical consistency among different variables<sup>73,81,82</sup>. All variables were unified to the same temporal (7 d) and spatial (0.5°) resolution, and the final upscaled dataset had the same spatiotemporal resolution as the inputting variables.

Additionally, we also used other sources of input datasets to assess the sensitivity of the temporal changes of wetland CH<sub>4</sub> emissions in the Boreal–Arctic during 2002–2021 to uncertainties in the input datasets. These additional datasets included University of East Anglia Climatic Research Unit Japanese Reanalysis<sup>83</sup>, Global Land Data Assimilation System<sup>84</sup>, Modern-Era Retrospective Analysis for Research and Applications v.2<sup>85</sup> and Penman–Monteith–Leuning GPP<sup>86</sup> datasets. More details of the datasets used and the sensitivity experiments are given in Supplementary Section 4.

### Wetland CH<sub>4</sub> emission observations

Substantial spatial heterogeneity of wetland CH<sub>4</sub> emissions has been highlighted in the literature<sup>7,41,48</sup>, and therefore sparse observations may impede reliable upscaling. To overcome this issue of spatial heterogeneity, we first compiled a comprehensive CH<sub>4</sub> dataset that broadly covered the Boreal–Arctic region, by combining the FLUXNET-CH4 dataset<sup>27</sup>, the BAWLD-CH4 dataset<sup>28</sup> and the chamber dataset in ref. 48. We selected all chamber sites that explicitly included the wetland types considered here and start and end months of the observations<sup>28,48</sup>.

We used quality-assured observed wetland CH<sub>4</sub> emissions at EC sites instead of gap-filled data. In total, this study included 139 and 168 site years of EC and chamber measurements, respectively. Detailed information (including site identifier, wetland type, location, temporal coverage, digital object identifier and references) on the sites is listed in Supplementary Tables 1 and 2. The compiled and upscaled dataset will be made available upon reasonable request.

### Causality-guided machine learning (Causal-ML) upscaling

A Causal-ML model<sup>7</sup> with good physical interpretability and accuracy was used for upscaling the wetland CH<sub>4</sub> emissions. The model first identified the causal relationships between each driver and CH<sub>4</sub> emission by excluding the confounding effects from other drivers through a PCMCI method<sup>7,87–90</sup> (PC refers to the model inventors, P. Spirtes and C. Glymour<sup>91</sup>, and MCI is the acronym for momentary conditional independence<sup>90</sup>). The PCMCI method has been frequently used in Earth science<sup>88,90,92–95</sup>, and is particularly suitable for inferring multivariate controlled and time-lagged causal relationships<sup>90,93–95</sup>, such as those between wetland CH<sub>4</sub> emission and its drivers<sup>7,8,47</sup> (see Supplementary Section 2 for more details of the causality inference). Then, the identified causal structures along with the model biases between observations and model simulations were used to guide model training. This modelling strategy helps reduce model biases and improve model physics<sup>7</sup>. Another benefit of this Causal-ML model is the representation of time-lagged controls, which has been shown to be important for understating and modelling wetland CH<sub>4</sub> dynamics<sup>7,13</sup>. Here, we considered the substantial intra-seasonal hysteresis found within wetland CH<sub>4</sub> emissions<sup>13</sup>, and differentiated the wetland-type-dependent CH<sub>4</sub> emission processes by building Causal-ML models for each wetland type. We randomly sampled 10% of site observations that the Causal-ML model had never seen as the testing dataset, and used the remaining 80% and 10% of the dataset to train and validate the model<sup>7</sup>, respectively. Through each experiment including data sampling and model training, we derived a Causal-ML model, and we repeated the experiments and upscaled the wetland CH<sub>4</sub> emission dataset 20 times. The ensemble mean of the 20 upscaled datasets was used to analyse the wetland CH<sub>4</sub> dynamics, and the s.d. was considered as the upscaling uncertainty related to trained model parameters caused by random data sampling. In addition, we also used the leave-one-out and temporal-cross-validation schemes for model evaluation and upscaling. For the leave-one-out scheme, we iteratively removed data from each site, retrained the model and then evaluated model performance<sup>7</sup>. For the temporal-cross-validation scheme, we used 20% and 80% of temporally continuous data for each site as the testing and training datasets, respectively. With the well trained models from the two additional validation schemes, we upscaled the wetland CH<sub>4</sub> emissions during 2002–2021. For high-frequency (that is, weekly, daily and hourly) measurements, the errors between modelled and observed wetland CH<sub>4</sub> emissions at the weekly scale were used in the objective function to direct the model training; for low-frequency (for example, some chamber observations only provided seasonal or annual-mean) measurements, the mean values of modelled and measured wetland CH<sub>4</sub> emissions during the observation period were compared and used in the objective function. Details of the model parameter settings, model training and validation are given in our previous work<sup>7</sup>.

### Identifying dominant controls on wetland CH<sub>4</sub> variability

To separate dominant controls on the inter-annual variations of wetland CH<sub>4</sub> emissions, we used a simple method of partial correlation<sup>92</sup>. We conducted analyses between CH<sub>4</sub> emission intensity and all input variables at the annual scale for each grid cell. Before the partial correlation analysis, the annual anomaly of each variable was derived by subtracting the long-term (2002–2021) annual mean and removing the inter-annual trend<sup>92</sup>. For each grid cell, the driver with the highest magnitude (absolute value) of partial correlation



coefficient was determined as the dominant driver. Finally, we classified all the drivers into four groups, including temperature (TS and TA), GPP, water-related factors (P and SWC) and others (WS, PA and SC). We acknowledge that the dependence of wetland CH<sub>4</sub> emissions on environmental predictors could vary across spatiotemporal scales<sup>8,49,96</sup>. Here we mainly focused on the dynamics of wetland CH<sub>4</sub> emissions at the inter-annual scale. At this scale, we found strong relationships between CH<sub>4</sub> emissions and environmental variables related to temperature, water and vegetation, consistent with previous studies<sup>27,49</sup>. We also acknowledge that these environmental variable dependences could vary over space, and become weaker when the dominant factors are beyond those considered in this study<sup>96</sup>. Due to spatial heterogeneity, we reported the dominant controls on the basis of the summary statistics of all wetland grid cells in the studied region with the CH<sub>4</sub> dynamics significantly explained by the considered environmental factors.

### Quantifying dominant controls on wetland CH<sub>4</sub> emission trend

Following previous studies<sup>97,98</sup>, a statistical linear regression model was used to quantify the controls from different drivers on the trend of wetland CH<sub>4</sub> emissions. In particular, we first built a linear model driven by all temporally changing input factors denoted Model<sub>all</sub>, to quantify the responses of wetland CH<sub>4</sub> emissions to environmental changes for each wetland grid cell. Then we iteratively held one group of factors, including temperature, GPP and water-related factors, constant at the corresponding initial level while allowing the other factors to change over time. For example, we used Model<sub>T</sub> to represent the model results that held temperature constant at 2002 values and allowed all the other factors to change over time. Similarly, we used Model<sub>GPP</sub> and Model<sub>water</sub> to represent the model results that kept GPP and water-related variables constant, respectively, while other factors varied over time. The differences ΔCH<sub>4</sub>(T), ΔCH<sub>4</sub>(GPP) and ΔCH<sub>4</sub>(Water) (equations (1)–(3)) were regarded as the impacts of changes in temperature, GPP and water-related variables on wetland CH<sub>4</sub> emission changes, respectively. The trend differences were regarded as the contributions from each group of factors to the increasing trend in wetland CH<sub>4</sub> emissions<sup>97,98</sup>. The model parameters (that is, the slope and intercept) for each grid cell were obtained by minimizing the sum of ordinary least squares of the errors<sup>53,54,99</sup>.

$$\Delta\text{CH}_4(T) = \text{Model}_{\text{all}} - \text{Model}_T = \beta_T \Delta T \quad (1)$$

$$\Delta\text{CH}_4(\text{GPP}) = \text{Model}_{\text{all}} - \text{Model}_{\text{GPP}} = \beta_{\text{GPP}} \Delta\text{GPP} \quad (2)$$

$$\Delta\text{CH}_4(\text{Water}) = \text{Model}_{\text{all}} - \text{Model}_{\text{water}} = \beta_{\text{water}} \Delta\text{Water}. \quad (3)$$

### Data availability

Data are available from the following sites: WAD2M, <https://zenodo.org/records/3998454>; BAWLD, <https://doi.org/10.18739/A2C824F9X> (ref. 72); GOSIF, <https://globalecology.unh.edu/data/GOSIF-GPP.html>; ERA5-Land, <https://www.ecmwf.int/en/forecasts/datasets/reanalysis-datasets/era5>.

### Code availability

The code used in this study is available at ref. 100.

### References

- Lehner, B. & Döll, P. Development and validation of a global database of lakes, reservoirs and wetlands. *J. Hydrol.* **296**, 1–22 (2004).
- Xi, Y. et al. Gridded maps of wetlands dynamics over mid–low latitudes for 1980–2020 based on TOPMODEL. *Sci. Data* **9**, 347 (2022).
- Prigent, C., Jimenez, C. & Bousquet, P. Satellite-derived global surface water extent and dynamics over the last 25 years (GIEMS-2). *J. Geophys. Res. Atmos.* **125**, e2019JD030711 (2020).
- Tootchi, A., Jost, A. & Ducharme, A. Multi-source global wetland maps combining surface water imagery and groundwater constraints. *Earth Syst. Sci. Data* **11**, 189–220 (2019).
- Li, X. & Xiao, J. A global, 0.05-degree product of solar-induced chlorophyll fluorescence derived from OCO-2, MODIS, and reanalysis data. *Remote Sens.* **11**, 517 (2019).
- Li, X. & Xiao, J. Mapping photosynthesis solely from solar-induced chlorophyll fluorescence: a global, fine-resolution dataset of gross primary production derived from OCO-2. *Remote Sens.* **11**, 2563 (2019).
- Li, X. et al. Solar-induced chlorophyll fluorescence is strongly correlated with terrestrial photosynthesis for a wide variety of biomes: first global analysis based on OCO-2 and flux tower observations. *Glob. Change Biol.* **24**, 3990–4008 (2018).
- Herrington, T. C., Fletcher, C. G. & Kropp, H. Validation of pan-Arctic soil temperatures in modern reanalysis and data assimilation systems. Preprint at *The Cryosphere Discuss.* <https://doi.org/10.5194/tc-2022-5> (2022).
- Li, M., Wu, P. & Ma, Z. A comprehensive evaluation of soil moisture and soil temperature from third-generation atmospheric and land reanalysis data sets. *Int. J. Climatol.* **40**, 5744–5766 (2020).
- Harris, I. *CRU JRA: Collection of CRU JRA Forcing Datasets of Gridded Land Surface Blend of Climatic Research Unit (CRU) and Japanese Reanalysis (JRA) Data* (Centre for Environmental Data Analysis (CEDA), 2019).
- Rodell, M. et al. The global land data assimilation system. *Bull. Am. Meteorol. Soc.* **85**, 381–394 (2004).
- Gelaro, R. et al. The Modern-Era Retrospective Analysis for Research and Applications, version 2 (MERRA-2). *J. Clim.* **30**, 5419–5454 (2017).
- Zhang, Y. et al. Coupled estimation of 500 m and 8-day resolution global evapotranspiration and gross primary production in 2002–2017. *Remote Sens. Environ.* **222**, 165–182 (2019).
- Yuan, K. et al. Deforestation reshapes land-surface energy-flux partitioning. *Environ. Res. Lett.* **16**, 024014 (2021).
- Yuan, K., Zhu, Q., Riley, W. J., Li, F. & Wu, H. Understanding and reducing the uncertainties of land surface energy flux partitioning within CMIP6 land models. *Agric. For. Meteorol.* **319**, 108920 (2022).
- Ruddell, B. L. & Kumar, P. Ecohydrologic process networks: 1. Identification. *Water Resour. Res.* **45**, W03419 (2009).
- Runge, J. et al. Inferring causation from time series in Earth system sciences. *Nat. Commun.* **10**, 2553 (2019).
- Spirtes, P., Glymour, C. N., Scheines, R. & Heckerman, D. *Causation, Prediction, and Search* (MIT Press, 2000).
- Li, F. et al. Wetter California projected by CMIP6 models with observational constraints under a high GHG emission scenario. *Earth's Future* **10**, e2022EF002694 (2022).
- Runge, J., Nowack, P., Kretschmer, M., Flaxman, S. & Sejdinovic, D. Detecting and quantifying causal associations in large nonlinear time series datasets. *Sci. Adv.* **5**, eaau4996 (2019).
- Runge, J. et al. Identifying causal gateways and mediators in complex spatio-temporal systems. *Nat. Commun.* **6**, 8502 (2015).
- Runge, J., Gerhardus, A., Varando, G., Eyring, V. & Camps-Valls, G. Causal inference for time series. *Nat. Rev. Earth Environ.* **4**, 487–505 (2023).
- Mastepanov, M. et al. Revisiting factors controlling methane emissions from high-Arctic tundra. *Biogeosciences* **10**, 5139–5158 (2013).

97. Yuan, W. et al. Increased atmospheric vapor pressure deficit reduces global vegetation growth. *Sci. Adv.* **5**, eaax1396 (2019).
98. Li, F. et al. AttentionFire\_v1. 0: interpretable machine learning fire model for burned-area predictions over tropics. *Geosci. Model Dev.* **16**, 869–884 (2023).
99. Andela, N. et al. A human-driven decline in global burned area. *Science* **356**, 1356–1362 (2017).
100. Yuan, K., et al. Boreal–Arctic wetland methane emissions modulated by warming and vegetation activity. *Zenodo* <https://zenodo.org/records/10525206> (2024).

## Acknowledgements

This research was supported by a NASA Carbon Monitoring System grant (NNH20ZDA001N) and the Reducing Uncertainties in Biogeochemical Interactions through Synthesis and Computation (RUBISCO) Scientific Focus Area Project; the latter is sponsored by the Earth and Environmental Systems Modeling (EESM) Program under the Office of Biological and Environmental Research of the US Department of Energy Office of Science. K.Y. is also supported by an Early Career Development Grant (ECDG), which was sponsored by the Earth and Environmental Sciences Area of Lawrence Berkeley National Laboratory.

## Author contributions

Q.Z conceived of the work and experiments; K.Y. and F.L. developed the model and conducted the analysis; K.Y., G.M., M.C., S.K., W.J.R. and R.J. prepared the data. All authors contributed to the writing.

## Competing interests

The authors declare no competing interests.

## Additional information

**Supplementary information** The online version contains supplementary material available at <https://doi.org/10.1038/s41558-024-01933-3>.

**Correspondence and requests for materials** should be addressed to Qing Zhu.

**Peer review information** *Nature Climate Change* thanks Torben Christensen, Lars Kutzbach and Jean-Daniel Paris for their contribution to the peer review of this work.

**Reprints and permissions information** is available at [www.nature.com/reprints](http://www.nature.com/reprints).